



HAL
open science

Unexpected diversity and ecological significance of uncultivable large virus-like particles in aquatic environments

Hermine Billard, Maxime Fuster, François Enault, Jean-François Carrias, Léa Fargette, Margot Carrouée, Perrine Desmares, Tom O Delmont, Estelle Bigeard, Gwenn Tanguy, et al.

► To cite this version:

Hermine Billard, Maxime Fuster, François Enault, Jean-François Carrias, Léa Fargette, et al.. Unexpected diversity and ecological significance of uncultivable large virus-like particles in aquatic environments. 2024. hal-04797458

HAL Id: hal-04797458

<https://hal.science/hal-04797458v1>

Preprint submitted on 22 Nov 2024

HAL is a multi-disciplinary open access archive for the deposit and dissemination of scientific research documents, whether they are published or not. The documents may come from teaching and research institutions in France or abroad, or from public or private research centers.

L'archive ouverte pluridisciplinaire **HAL**, est destinée au dépôt et à la diffusion de documents scientifiques de niveau recherche, publiés ou non, émanant des établissements d'enseignement et de recherche français ou étrangers, des laboratoires publics ou privés.

1 Unexpected diversity and ecological significance of uncultivable 2 large virus-like particles in aquatic environments

3
4 Hermine Billard, Maxime Fuster, François Enault, Jean-François Carrias, Léa Fargette,
5 Margot Carrouée, Perrine Desmares, Tom O. Delmont, Estelle Bigeard, Gwenn Tanguy,
6 Pauline Nogaret, Anne-Claire Baudoux, Urania Christaki, Téléphore Sime-Ngando, Jonathan
7 Colombet*

8 9 Abstract

10 The discovery of Jumbo phages and giant viruses of microeukaryotes has transformed our
11 perception of the virosphere. Metagenomic and metatranscriptomic data further highlight their
12 diversity and ecological impact. Nevertheless, sequence-based approaches fail to take into
13 account the morphological diversity of non-cultivated viruses, resulting in our fragmented
14 understanding of their nature and role in the environment. Here, we combined flow cytometry
15 and electron microscopy to uncover both previously unsuspected morphological diversity as
16 well as significant abundances of large viruses in aquatic environments. We discovered four
17 new viral morphotypes, all of which were associated with microeukaryotes. We also obtained
18 insights into the multi-year dynamics of the abundances of both giant microeukaryotic viruses
19 and Jumbo phages. This work deepens our understanding of large viruses and reveals their key
20 role as regulators of microbial communities.

21 22 Introduction

23 Viruses are major actors in the environment, affecting microbial community structure and
24 biogeochemical cycles¹⁻⁴. Viruses forming large particles (above 0.2 μm) that infect unicellular
25 algae⁵ or bacteria, referred to as “Jumbo” phages⁶, have been known for several decades.
26 However, they only came to prominence following the discovery of so-called “giant” viruses
27 (up to 1.5 μm), including the iconic mimiviruses and pandoraviruses. These giant viruses,
28 obtained mainly by the cultivation of *Acanthamoeba polyphaga* or algal species⁷⁻¹⁰, have had
29 a dramatic impact on our understanding of the evolution of viruses and blurred the boundaries
30 between viruses and cells in terms of their physical dimensions and genomic complexity.

31 These culture-based studies enabled the detailed genotypic-phenotypic and biological
32 characterization of isolated virus-host pairs^{5,6,11,12}. However, the isolation of viruses is
33 hampered by our limited ability to cultivate most microbes such as heterotrophic
34 microeukaryotes¹³, let alone their viruses.

35 Metagenomics has allowed us to progressively uncover many new giant virus genomes,
36 demonstrating that these viruses are present and diverse in most ecosystems^{2,14-18}.
37 Metagenome-assembled genomes (MAGs) can ascertain their genomic diversity, clarify their
38 taxonomy^{19,20}, and highlight their role in the evolution of cellular life forms²¹⁻²³. For example,
39 tens of MAGs were shown to form a diversified and prevalent group of viruses, representing a
40 potential new phylum known as *Mirusviricota* related to the herpesviruses²⁴. However, MAGs

41 of giant viruses are often incomplete, containing little or no information about the important
42 biological and ecological features such as the host range, mode of infection, absolute
43 abundance, or structure and composition of the viral particle. Metatranscriptomics can provide
44 additional information by pointing to the host of giant uncultured viruses or accessing their
45 activity within these hosts²⁵. However, as with metagenomics, this approach does not provide
46 access to the structure and composition of viral particles or to demonstrate their absolute
47 abundances.

48 To tackle the limitations of both culture and omics-based studies, Fischer et al.²⁶ recently used
49 transmission electron microscopy (TEM) to complement metagenomic approaches, thus
50 revealing the surprising structural diversity of giant virus-like particles (VLPs) in forest soils.
51 Although this methodology allows us to identify and categorize giant viruses based on
52 morphological criteria, it is time-consuming and difficult to apply at high throughput.
53 Consequently, this methodology alone is not well suited to tracking viral dynamics, thus
54 preventing a better comprehension of the functional role played by viruses in natural
55 ecosystems.

56 Flow cytometry (FC) is a rapid and inexpensive method that can be used to characterize
57 environmental samples, leading to the absolute enumeration of nano- and microparticles. FC
58 proved to be highly valuable for monitoring known viruses, mainly algal²⁷⁻³⁰, but also viruses
59 grouped into cytometric populations characterized by specific diffusion and fluorescence
60 signals³¹⁻³³. However, at the current stage and in the absence of a specific marker for large
61 viruses, the composition of these cytometric populations in environmental samples remains
62 uncertain, even in terms of their morphology.

63 The recently developed FC sorting of viruses offers new perspectives to fill the gap between
64 genotypic/morphological data and ecological significance, as it can provide absolute counts of
65 characterized viruses after sorting. Nevertheless, to date, the application of FC sorting has
66 remained limited to cultivable viruses³⁴ or genomic characterizations³⁵⁻³⁸.

67 For the detection, morphological characterization, and ecology of large aquatic VLPs, we
68 developed a strategy coupling TEM and FC. Applying this strategy in both directions (i.e.,
69 FC→TEM and TEM→FC) provides valuable information about large VLPs, regardless of
70 whether they are labeled with a specific dye.

71 These methodological developments allowed us (i) to characterize a considerable diversity of
72 large VLPs in three French lakes, including four new types that probably infect unicellular
73 eukaryotes and (ii) to provide insights into the dynamics and ecology of their populations.

74

75 **Methods**

76 **Study sites and sample collection**

77 Samples were collected at the surface (0-40 cm) of three artificial freshwater lakes: Fargette
78 (45°44'39''N; 3°27'21''E; 465 m altitude; surface area 1.2 ha; maximum depth 2.5 m), Saint
79 Gervais d'Auvergne (SG) (46°02'15''N; 2°48'43''E; 680 m altitude; surface area 10.5 ha;
80 maximum depth 4.5 m), and Chambon (45°50'22''N; 3°30'17''E; 490 m altitude; surface area
81 1.2 ha; maximum depth 6 m). These lakes are located within a 120 km radius in the French
82 Massif Central. Fargette is a hyper-eutrophic lake, while SG and Chambon are eutrophic lakes

83 with a significant human presence (leisure, fishing, swimming, etc.). At regular intervals, we
84 sampled Lake Fargette from December 21, 2020, to January 18, 2024, Lake SG from February
85 13, 2020, to January 18, 2024, and Lake Chambon from March 23, 2022, to January 18, 2024,
86 sampling a total of 86, 104, and 62 time points, respectively.

87 Samples for the counts and determination of virus-like particles (VLPs), prokaryotes (FC,
88 TEM), and autotrophic/heterotrophic eukaryote communities (by light microscopy) were
89 immediately fixed with 1% (v/v) formaldehyde and stored at 4°C until analysis. Unfixed
90 samples for the analysis of autotrophic/heterotrophic eukaryote communities by FC and for
91 diversity analysis were transported at 4°C and treated in the 4 hours following sampling.

92 Marine samples were also collected from North Atlantic waters during the APERO expedition
93 onboard *Pourquoi Pas?* in June and July 2023. One-liter volumes were collected from Nisking
94 bottles at a depth of 2, 20, and 200 m at the three stations (PSS1: 48°27,167 N; 22°30,059 W,
95 PSS2: 50°37,250 N; 19°7,098 W, PSS3: 47°49,846 N; 15°46,690 W). The water was prefiltered
96 through 1.2 µm glass-fibers filters (GFC Whatman) and concentrated 9- to 10-fold by
97 ultrafiltration using a 0.2 µm cartridge (PES Vivaflow, Sartorius). An 8 mL aliquot of the
98 concentrate was fixed with EM grade glutaraldehyde (2% final concentration), flash frozen, and
99 stored at -80°C until analysis.

100

101 **Abiotic parameter measurements**

102 Dissolved oxygen content (mg.L⁻¹) and temperature (°Celsius) were measured *in situ* with a
103 submersible probe (ProDSS YSI, Yellow Springs, Ohio, USA).

104

105 **Biotic parameter analysis**

106 *Total pigment analysis (probe) and phytoplankton count (flow cytometry)*

107 Total pigment content was measured (µg.L⁻¹) using a submersible spectrofluorometric probe
108 (BBE FluoroProbe, Moldaenke GmbH, DE) directly placed in the lake. Counts of pico- and
109 nanophytoplankton populations (green algae, Cyanobacteria, Cryptophyta) were determined by
110 FC using a BD LSR Fortessa X-20 (BD Sciences, San Jose, CA). Autotrophic organisms were
111 categorized into five subpopulations (three subpopulations of green algae, Cyanobacteria, and
112 Cryptophyta) according to their pigment content. Fluorescence signals from chlorophyll,
113 phycoerythrin, and phycocyanin were collected using 405nm (50mW), 561nm (50mW), and
114 640nm (40 mW) lasers and 670/30, 586/15, and 670/14 filters, respectively. Green algae
115 correspond to cells containing only chlorophyll. Cyanobacteria is the sum of phycoerythrin-
116 and phycocyanin-rich cyanobacteria (here, we combined picocyanobacteria and large
117 cyanobacteria). Finally, Cryptophyta corresponds to populations whose main pigments are
118 phycoerythrin and chlorophyll.

119

120 *Total (auto-/heterotrophic) microeukaryote counts (flow cytometry)*

121 Counts of total (auto-/heterotrophic) microeukaryotes from unfixed samples were performed
122 by FC using a BD LSR FORTESSA X-20 (BD BioSciences, San Jose, CA USA). The term

123 “microeukaryote” used in this manuscript refers to unicellular planktonic eukaryotes detectable
124 in FC or light microscopy, without size criteria.

125 First, autotrophic cells were targeted according to the autofluorescence of their chlorophyll
126 content (405 nm, 50mW laser, and 635 longpass – 670/30 bandpass filters). At this stage,
127 untargeted cells are considered heterotrophic. In each of these two populations
128 (auto/heterotrophic), eukaryotic cells were pre-selected based on their granularity and dsDNA
129 content using the Sybr Green I (SGI) dye (488 nm, 60 mW laser, and 502 longpass – 450/50
130 bandpass filters). Finally, eukaryotic heterotrophic cells were defined by mitochondrial
131 membrane staining with 200 μ M Biotracker 405 Blue Mitochondria Dye (SCT135, Sigma-
132 Aldrich, MERCK KGaA) (405 nm, 50 mW laser, and 450/50 bandpass filter). Total
133 microeukaryotes are the sum of auto- and heterotrophic cells. This strategy assumes that all the
134 cells of interest have mitochondria. All cytometric data were acquired and analyzed with BD
135 FACSDiva 9.0 software.

136

137 *Community composition of auto- and heterotrophic microeukaryotes (light microscopy)*

138 The community composition of microeukaryotes, including eukaryotic algae, heterotrophic
139 flagellates, and ciliates, was assessed by light microscopy. Subsamples of 1 to 4 ml (taken from
140 the 1% formaldehyde-fixed samples) were inoculated in Utermöhl’s settling chambers
141 containing 10 ml of < 2 μ m-distilled water to ensure a proper dispersion of the settled cells on
142 the slide. The next day, slides were examined and counted under inverted epifluorescence
143 microscopy (Zeiss Axiovert 200M, Carl Zeiss company, Oberkochen, Germany) from
144 randomly selected transects. Cells were visualized at x400 magnification and pigmented taxa
145 were distinguished by detecting the autofluorescence of chlorophyll a and phycoerythrin under
146 blue light (450–490 nm) and green light (520–560 nm) excitation, respectively. All the taxa
147 were identified with respect to their size, shape, and specific morphological characteristics (e.g.,
148 presence of flagella or cilia, colonial forms, autofluorescence, shell) to the lowest possible
149 taxonomic level.

150 Net microeukaryote production (NMP) was quantified as the difference in total microeukaryote
151 abundance (determined by FC or light microscopy) between time N and time N-1 divided by
152 the elapsed time.

153

154 *Diversity of eukaryotes (18S metabarcoding analysis)*

155 For a selection of unfixed samples, microbial communities were collected on a 0.2- μ m
156 polycarbonate filter (Millipore) (until saturation, pressure < 25 kPa) and stored at –20°C until
157 DNA extraction. The filters were covered with a lysing buffer (lysozyme 2 mg ml⁻¹, SDS 0.5%,
158 Proteinase K 100 μ g mL⁻¹, and RNase A 8.33 μ g mL⁻¹ in TE buffer pH 8) at 37°C for 90 min.
159 A CTAB 10% / NaCl 5 M solution was added, and the samples were incubated at 65°C for 30
160 min. Nucleic acids were extracted with phenol–chloroform–isoamyl alcohol (25:24:1); the
161 aqueous phase containing the nucleic acids was recovered and purified by adding chloroform-
162 isoamyl alcohol (24:1). Nucleic acids were then precipitated with a mixture of glycogen 15 μ g
163 mL⁻¹, sodium acetate 0.1M, and ethanol 100% overnight at –20 °C. The DNA pellet was rinsed
164 with ethanol (70%), dried, and dissolved in the TE buffer. DNA was then purified using a

165 commercial kit (NucleoSpin® gDNA Cleanup, Macherey-Nagel) and quantified by Qubit
166 dsDNA HS kit.

167 The V4 region of the eukaryote SSU RNA gene was amplified using the TAREuk454FWD1
168 (5'-CCAGCASCYGC GGTAATTCC-3') and TAREukREV3 (5'-
169 ACTTTCGTTCTTGATYRA-3') primers tagged with adaptors as recommended by the
170 sequencing platform. Each polymerase chain reaction (PCR) was performed in a total volume
171 of 50 µL containing 1 × final reaction buffer, 2 mM MgCl₂, 0.2 mM dNTP, 250 µg mL⁻¹ BSA,
172 0.4 µM each primer, 1.25 U GoTaq® Flexi DNA Polymerase (PROMEGA), and 20 ng DNA
173 template. The PCR protocol used an initial activation step at 94°C for 1 min, followed by 12
174 “three-step” cycles consisting of 94°C for 10 s, 53°C for 30 s, and 72°C for 30 s, followed by a
175 further 18 “three-step” cycles consisting of 94°C for 10 s, 48°C for 30 s, and 72°C for 30 s, and
176 a final 10-min extension at 72°C. PCR products were purified on agarose gel with Nucleospin®
177 Gel and the PCR clean-up kit (Macherey-Nagel) and quantified using the Qubit dsDNA HS kit.

178 Library preparation, sequencing (on Illumina MiSeq, v3, 2*300 cycles), and metagenomic
179 bioinformatic analysis (reference database: <https://pr2-database.org/>) were performed by the
180 sequencing platform (Microsynth, Switzerland).

181

182 *Quantification of labeled large dsDNA virus-like particles (Fig. 1A, Step 1a FC→TEM) and*
183 *prokaryotes*

184 Counts of dsDNA VLPs and prokaryotes from fixed samples were performed in triplicates by
185 FC using the dsDNA SYBR Green I (SGI) dye (S7585, Invitrogen, Thermo Fisher Scientific)
186 according to Brussaard (2004)²⁹ with a BD FACSAria Fusion SORP (BD Sciences, San Jose,
187 CA, USA) equipped with an air-cooled laser delivering 50 mW at 488 nm with 502 longpass,
188 and 530/30 bandpass filter set-up. All cytometric data were acquired and analyzed with BD
189 FACSDiva 9.0 software.

190 Microbial and VLPs were divided into subpopulations according to their intensity on the side
191 scatter (SSC) and SGI signals. First, prokaryotes were targeted. Second, two populations (VLP1
192 and VLP2) were characterized by low SSC and/or low SGI signals. VLP1 is dominated by small
193 bacteriophages (< 200 nm)^{29,39}, although small eukaryotic algal viruses such as small genome-
194 sized *Heterosigma* or diatom viruses can also display similar low fluorescence signatures^{40–43}.
195 VLP2 was mainly composed of tailless icosahedra of around 100 nm in diameter (data not
196 shown), commonly identified as dsDNA algal viruses^{28,41,44}. Between these microbial and small
197 VLP populations, four populations were identified on cytograms characterized by high SSC
198 and/or high SGI signals. Considering the morphology of the VLPs contained therein (observed
199 and regularly verified after FC sorting by TEM), these four populations were named Jumbo
200 (Jumbo-like phage), Shield, Ham, and giant icosahedral VLPs (GIV).

201 Jumbo, Shield, Ham, and GIV form a group of large dsDNA VLPs.

202 The gating and counting strategy are provided in **Fig. 1A**. Gates with gate overlaps, notably
203 from prokaryotes or debris populations, were excluded from the analysis.

204 Note that we were unable to identify cytometric populations corresponding to Snake and Sword
205 VLPs on cytograms after FC sorting. For these populations, only TEM→FC counts were
206 available (**Fig. 1B**).

207

208 *Fluorescence-activated large virus-like particle sorting (Fig. 1A, Step 1b FC→TEM)*

209 For VLP sorting, we selected dates with remarkable virus populations on account of their
210 fluorescence signals and intensity: Fargette on March 1, 2022, SG on February 14, 2022, and
211 Chambon on December 16, 2022, and January 12, 2024.

212 VLP sorting (1% formaldehyde-fixed sample) was performed with the FACSAria Fusion SORP
213 (BD Biosciences, San Jose, CA, USA) flow cytometer using a 488 nm argon laser for excitation.
214 The “single cell” sort mode was used to ensure that the sorted drops were free of contaminating
215 particles and that the target particles were centered within the deflected drop.

216 Sorting instruments and reagents were decontaminated as recommended by the manufacturer
217 (Prepare for Aseptic Sort, BD Biosciences, San Jose, CA, USA). The threshold of the cytometer
218 was triggered at the minimum in the green fluorescence channel, and the sorting gates were
219 based on SGI fluorescence and SSC.

220 From each of the distinct populations mentioned above, between 3.10^5 and 3.10^6 VLPs were
221 sorted for TEM identification. For this sorting, we used sterile NaCl ($2.24\text{g}\cdot\text{L}^{-1}$) diluted in
222 ultrapure water solution as sheath fluid. This NaCl concentration was determined to permit
223 correct deflection (concentration range test, data not shown) in order to prevent salt
224 contamination of the TEM observations.

225

226 *Quantification of specific large virus-like particles with or without flow cytometry signal (Fig.*
227 *1B, Step 1 and 2 TEM→FC) and morphological characterization (Fig. 1A Step 2, 1B Step 1)*

228 VLPs and microbial communities in 1% (v/v) formaldehyde fixed samples were collected by
229 centrifugation at $20,000 \times g$ for 20 min at 14°C directly on 400-mesh electron microscopy
230 copper grids covered with carbon-coated Formvar film (AO3X, Pelanne Instruments, Toulouse,
231 France). Particles were over-contrasted using uranyl salts. Specific viruses were detected,
232 characterized, and counted by TEM using a Jeol JEM 2100-Plus microscope (JEOL, Akishima,
233 Tokyo, Japan) equipped with a Gatan Rio 9 CMOS camera (Gatan Inc., Pleasanton, USA)
234 operating at 80 kV and $\times 50,000$ to $\times 150,000$ magnifications. TEM images were acquired and
235 measurements made with DigitalMicrograph-GMS 3 (Gatan Inc., Pleasanton, USA). Resizing
236 as well as light and contrast corrections were carried out with ImageJ⁴⁵ or Photos Microsoft
237 (Microsoft Corporation, Redmond, Washington, USA). Scale bars were retraced and formatted
238 manually.

239 The number of specific VLPs with (Ham, Shield) or without FC signals (Snake and Sword)
240 resulted from the multiplication of the VLP/prokaryote ratio determined by TEM by the
241 prokaryote concentration obtained by FC (**Fig 1B, Step 2 TEM→FC**).

242 The terms “large,” “Jumbo,” or “giant” were used in relation to the size of VLPs (length >200
243 nm on one of their axes) and FC characteristics (high values of SGI (dsDNA) or SSC
244 (complexity/size) mean fluorescence intensities).

245 For VLPs presenting an identified cytometric population (Shield, Ham), we validated the
246 reciprocity between the methods FC→TEM and TEM→FC by their positive correlation
247 (**Extended Data Fig. 1**). In the analysis of their dynamics, we present the results of the method
248 with the maximum number of points (i.e., FC→TEM for Shield VLPs and TEM→FC for Ham
249 VLPs). Giant icosahedral VLPs were only counted by FC. For VLPs with no detectable
250 cytometric signature using SGI (Snake and Sword), the TEM→FC approach was the only
251 methodology permitting the detection, identification, and quantification of VLPs in this study.

252 Large dsDNA VLP populations (Shield, Ham, Giant Icosahedral, Jumbo-like phages, Snake
253 and Sword VLPs) were combined to consider the total community of large VLPs. Jumbo-like
254 phages were removed to consider the potential population of large microeukaryote VLPs.

255 Net viral production was quantified for each large VLP and for the sum of large microeukaryote
256 VLPs as the difference in VLP abundance between time N and time N-1 divided by time. A
257 theoretical viral death rate of microeukaryotes was evaluated as the net viral production divided
258 by the burst size (BS). BS was determined from TEM observations of host lytic events for
259 Shield, Ham, Snake, and Sword VLPs. For GIV, we used a theoretical BS of 50. For the total
260 large microeukaryote VLPs, we used the average of the BS observed in TEM and in theory for
261 each of the quantified viral types. We considered the estimate of the viral death rate of
262 microeukaryotes to be minimal, as it does not take into account the viral decay, which was not
263 measured here (**Table 1A**).

264 We estimated the removal of NMP by large microeukaryote VLPs by applying the ratio between
265 the viral death rate of microeukaryotes and NMP. It was only estimated at the dates for which
266 autotrophic and heterotrophic microeukaryote counts by light microscopy or mitochondrial
267 tagging were available (**Table 1B**).

268

269 **Data analysis**

270 All statistical analyses were performed using R software (version 4.1.3, R Foundation for
271 Statistical Computing, Vienna, Austria). Potential relationships among all variables were tested
272 by pairwise correlations (Spearman correlation analyses).

273

274 **Results and discussion**

275 **Large VLPs: Abundant and dynamic players in viral ecology**

276 Data from cultures^{5,6,10–12}, microscopic observations²⁶, and genomic analyses^{2,14–17} have led to
277 fundamental discoveries in the study of large viruses. However, in the absence of a
278 methodology to detect, characterize, and quantify their non-cultivable representatives, their
279 diversity and ecological importance remains underexplored. To fill this knowledge gap, we
280 coupled FC and TEM (**Fig. 1**) to study large viral particles in aquatic ecosystems. FC not only
281 allowed the detection and absolute counts of large VLPs²⁹ carrying dsDNA genomes

282 fluorescently labeled with SYBR Green I (SGI) but also enabled the comparison of
283 corresponding subpopulations on the basis of fluorescence signals associated with SSC and
284 dsDNA fluorescence^{28,31,34} (**Fig. 1A**). TEM allowed us to assess the homogeneity and
285 morphological characteristics of the populations sorted using FC as well as the visualization
286 and quantification of large VLPs (**Fig. 1A-B**) from environmental samples that were not labeled
287 in the FC analysis.

288 Using this protocol, the populations of large VLPs were morphologically characterized and
289 quantified in multiple samples collected at regular intervals over successive years (2020-2024)
290 in three artificial eutrophic freshwater lakes located in the French Massif Central (Lakes
291 Fargette, Saint Gervais d’Auvergne (SG), and Chambon).

292 Large VLPs (FC labeled or not) were consistently present in the studied systems, with
293 abundances ranging from 0.02 to 2.8×10^7 VLPs.mL⁻¹, i.e., from 0.2 to 11.2% of total VLPs.
294 Their dynamics were characterized by phases of production in spring or late autumn alternating
295 with low detection phases (**Fig. 2**). Notably, among the large VLPs, up to 78% were unlabeled
296 (**Fig. 2**). To decipher the significance of aquatic large VLPs, most of which did not resemble
297 the previously characterized VLPs, we explored their morphological diversity and ecological
298 patterns (i.e., dynamic, interactions with microbial communities) while separating the VLPs
299 into two groups, namely Jumbo phages and large VLPs likely associated with microeukaryotes.
300 The term “microeukaryotes” used in this manuscript refers to unicellular planktonic eukaryotes
301 detectable in FC or light microscopy, irrespective of their size.

302

303 **Overlooked diversity and ecological significance of Jumbo phages**

304 Although a number of Jumbo phages were previously isolated and cultivated^{11,46}, their diversity
305 and ecology in aquatic environments were almost exclusively analyzed by metagenomics^{2,16}.
306 These studies uncovered an enormous diversity, suggesting that Jumbo phages are important,
307 yet underestimated components of microbial communities and food webs². To examine this
308 viral component, we identified a specific cytometric population that corresponds to Jumbo-like
309 phages, as confirmed by TEM observations following FC sorting (**Fig. 3A-B**). The population,
310 named Jumbo, was characterized by a low SSC and a high level of fluorescence, which is a
311 proxy for the large genome sizes of Jumbo phages (> 200 kb) and consistent with what was
312 previously demonstrated for the iconic Jumbo coliphage T4²⁹. TEM showed capsid sizes
313 between 90 and 110 nm in diameter, with total lengths between 270 and 467 nm (**Fig. 3B-C**).
314 The overall organization of VLPs was characterized by head-tailed phages of the class
315 *Caudoviricetes*¹¹. The abundances of the Jumbo VLPs reached 7.9×10^6 VLPs.mL⁻¹, and their
316 dynamics showed irregular phases of development (**Fig. 3D**). For example, there was a
317 noticeable peak in Lake SG from March 8 to July 4, 2022. Jumbo VLPs were detected in all the
318 years under investigation. As expected, this population showed a positive correlation with
319 prokaryotes ($R^2 = 0.63$, p-value < 0.00001).

320 In the absence of evident burst events, we used a theoretical BS of 50, within the range of a
321 previous report⁴⁷, to estimate the high maximum potential mortality of 1.1×10^7 hosts.L⁻¹.day⁻¹
322 (**Table 1A**).

323 The potential Jumbo phages observed in the raw environmental samples (**Fig. 3C and**
324 **Extended Data Fig. 2**) were more morphologically diverse than those belonging to the Jumbo

325 population sorted by our defined cytometric gate. Indeed, whereas the VLPs of the Jumbo FC
326 population were fairly homogeneous in shape and size, environmental Jumbo-like VLPs tended
327 to be more heterogeneous. Although some particles consisted of a well-defined capsid and tail,
328 others had tails that were covered by complex sheath-like structures or that were remarkably
329 long, up to 2,200 nm in length. Even though we cannot exclude the possibility that all these
330 diverse tailed particles were in our defined Jumbo cytometric gate, most were likely rare and
331 outside any cytometric gate.

332 These results show that Jumbo-like phages are neglected in the aquatic environment in terms
333 of their diversity, abundance, and induced mortality. Indeed, that they could be of major
334 importance in the microbial loop².

335

336 **Large VLPs of microeukaryotes: Amazing diversity and unexpected ecological** 337 **significance**

338 As in the case of Jumbo phages, the diversity and ecology of large aquatic VLPs of
339 microeukaryotes remains largely underexplored. Here, we discovered four new abundant large
340 viral morphotypes. Whereas VLPs resembling the Shield form were previously detected in soil
341 samples, dubbed as the “Christmas star”²⁶, the Ham, Snake and Sword VLPs present completely
342 new shapes never before observed. In addition, we provide the morphological characterization
343 and monitoring of abundant large icosahedral VLPs and highlight the ecological significance
344 of the total community of large VLPs of microeukaryotes.

345

346 *Ham virus-like particles: Atypical morphology of a new viral type*

347 During our study, we detected a particular cytometric signature corresponding to a new type of
348 VLPs, which we named Ham. The average fluorescence intensities derived from the dsDNA
349 labeling and SSC of these particles were intermediate, being situated between VLPs2 and
350 prokaryotes, suggesting that they have large genomes (**Fig. 1A, 4A**).

351 The Ham VLP is a polymorphic particle with lengths ranging from 450 to 1070 nm (**Fig. 4**). It
352 is characterized by an ovoid head ranging from 240 to 500 nm in length and from 135 to 190
353 nm in width, a tail surrounded by an apparently helical assembly ranging from 140 to 550 nm
354 in length and from 40 to 50 nm in width. The end of the tail is decorated by fibers. Some
355 morphotypes have a bulge at the end of the tail. A notable feature is the presence of an
356 icosahedral structure of 75-80 nm in diameter inside the head. The reproducibility of the
357 observations of this icosahedral structure inside the putative virion suggests that this is an
358 integral part of the Ham VLP. Two or three icosahedrons inside the largest form were
359 occasionally observed (**Fig. 4B**). These multi-icosahedron forms were rare (< 1%), except in
360 Lake Chambon from December 20, 2023, to January 10, 2024, in which they could represent
361 up to 64% of the total Ham VLPs counted. To our knowledge, this is the first description of a
362 head-tail VLP with an icosahedral structure covered by an external layer. Morphologically, the
363 closest relative appears to be the enigmatic virions of Meelsvirus, which have head-tail particles
364 with the head containing an ovoid nucleocapsid⁴⁸.

365 Ham VLPs were encountered in all three lakes considered in this study and reached 3.1×10^6
366 VLPs.mL⁻¹ with a sudden and massive development strategy (**Fig. 4C**). The proliferation

367 dynamics of Ham VLPs strongly correlated with the FC phytoplanktonic microeukaryote
368 population identified as Cryptophyta ($R^2 = 0.3$, p -value < 0.00001). Metabarcoding data showed
369 that at the time of the VLP bloom, eukaryotic communities were dominated by Cryptophyceae,
370 which further suggests that Ham VLPs are produced by the Cryptophyceae species (**Fig. 4D**).
371 Notably, the interaction between Ham VLPs and autotrophic microeukaryotes was also
372 supported by the “prey-predator” model (**Fig. 4D**). This model of interaction has been
373 frequently observed for large algal viruses^{33,49–53}. Without further precisions about the specific
374 identity of the host, these observations suggest that Ham VLPs infect autotrophic
375 microeukaryotes. The pleomorphism of Ham VLPs suggests that it could be represented by
376 different phylotypes, a possibility reinforced by the ubiquity of Ham VLPs and their
377 development at different times of the year under contrasting environmental conditions
378 (temperature range 5 to 20 °C). However, its development strategy and malleable morphology
379 could also support the hypothesis of specific polymorphic VLPs.

380 The small number of VLPs counted after the observation of cell remnants (**Fig. 4E**) suggests
381 that the BS was reduced to a few units. We estimated this VLP to be involved in the mortality
382 of up to 2.9×10^7 hosts.L⁻¹.day⁻¹ (**Table 1A**).

383

384 *Shield virus-like particles: A new universal viral phylum?*

385 Like Ham VLPs, Shield VLPs exhibited a specific cytometric signature with fluorescence
386 intensities in the range of small prokaryotes and slightly lower than Jumbo-like phages. The
387 cytometric signatures of Ham and Shield VLPs correspond those of large genome dsDNA algal
388 viruses such as *Phaeocystis* or *Emiliana huxleyi* viruses^{27–31} or *Bodo saltans* virus infecting a
389 heterotrophic flagellate⁵⁴, suggesting a large genome (**Fig. 1A, 5A**).

390 Shield VLPs have an electron-dense inner capsid (140–300 nm in diameter) surrounded by a
391 less electron-dense spherical outer structure (194–460 nm in diameter) (**Fig. 5A-B, Extended**
392 **data Fig. 3A**). The inner capsid features a pentagonal planar projection with a 5–9 nm thick
393 border. Some representatives of Shield VLPs suggest that the external structure is composed of
394 a tegument and an envelope, as is characteristic of viruses in the order *Herpesvirales* (**Fig. 5B**).
395 However, the nature of this envelope-like structure is unclear, as it could be lipidic, as in
396 herpesviruses, or based on glycans, as in *Megavirinae*^{55,56}. Unlike *Megavirinae*, the hairy
397 appearance resulting from the arrangement of fibrils has not been clearly observed, and some
398 Shield representatives listed here are smaller than *Megavirinae*. However, one example of a
399 particular *Megavirinae*, namely Cotonvirus (400 nm in capsid diameter), shows that the density
400 of fibrils on the capsid can have a smooth appearance under TEM⁵⁷.

401 We observed cells from different types infected with Shield VLPs: amoeboid forms 3 μm in
402 diameter and different types of flagellated microeukaryotes with a head ranging from 1.8 μm
403 to 6 μm with one or two flagella (**Fig. 5D, Extended data Fig. 3B**). The nature of their hosts
404 and their auto- and/or heterotrophic trophic mode remain to be determined. However, some of
405 them did not exhibit or lacked pigment content under fluorescence microscopy. This putative
406 broad host range was also suggested by positive correlations between Shield VLPs and almost
407 all the microbial compartments mentioned above (p -value < 0.01). We assumed that Shield
408 VLPs infect flagellated heterotroph microeukaryotes. Indeed, very rare large viruses such as
409 *Cafeteria roenbergensis* virus⁵⁸ and Klosneuviruses^{54,59}, which are capable of infecting them,

410 have been morphologically described⁶⁰, and no ecological description (*in situ* temporal or
411 spatial dynamic) is available. Shield VLPs are ubiquitous and were encountered in all three
412 lakes studied here. We quantified Shield VLPs with remarkable abundances reaching $13.7 \times$
413 10^6 VLPs.mL⁻¹ and with a dynamic characterized by irregular phases of development (**Fig. 5C**).

414 With an observed mean BS of 27 (**Fig. 5D, Extended data Fig. 3B**), we estimated Shield VLPs
415 to be involved in the mortality of 1.3×10^7 hosts.L⁻¹.day⁻¹ (**Table 1**).

416 The ubiquitous distribution of Shield VLPs, which developed at different times of the year
417 under contrasting environmental conditions, was reinforced by our observations of numerous
418 Shield morphotypes in marine systems in which they can reach 8.3×10^4 VLPs.mL⁻¹ in surface
419 area (**Extended data Fig. 3C**) as well as by their previous observation in soils²⁶. Coupled with
420 the pleomorphism of Shield VLPs and its potential host range, we suggest that this could
421 represent a new generalist phylum, not considered until now, which plays a major ecological
422 role in the regulation of microeukaryotes in many environments.

423 Finally, we also recorded striking rare forms of Shield-like VLPs (less than 1% of our
424 observations) bearing tails or fibrils or in tandem (**Extended data Fig. 4**), up to 600 nm in
425 diameter. We cannot certify the presence of these tail forms in the cytometric gate
426 corresponding to the Shield VLPs.

427

428 *Giant icosahedral virus-like particles: Novelties in common large viruses*

429 This population, sorted by FC and verified by TEM, corresponded to giant icosahedral VLPs
430 (GIV) (**Fig. 6A**). Like Ham and Shield VLPs, their cytometric signature suggested a large
431 genome. A particular feature was their high signal on fluorescence associated with SSC,
432 suggesting high internal complexity (**Fig. 1A, 6A**).

433 In this population, three morphotypes were observed: (i) tailless naked giant icosahedron (79%
434 of the population in Chambon on January 10, 2024) of 212 nm in diameter; (ii) tail giant
435 icosahedron (20%) of 180 nm in diameter with a tail of 150 nm length; and (iii) fibrils bearing
436 giant icosahedron (< 1%) of 230 nm in diameter (**Fig. 6A**). The morphologies and sizes of the
437 first two groups are similar to those observed for members of the *Megaviricetes* class, whereas
438 no affiliation was proposed for the observed tailed types. Illustrations of various tailed GIV are
439 provided in **Fig. 6B**. Finally, we also reported rare (less than 1% of the GIV observations) and
440 GIV with a saccule (up to 446 nm icosahedral diameter) and morphotypes with tubular
441 appendages (**Fig. 6B**) previously recorded in forest soils as “Gorgon”²⁶. We cannot certify the
442 presence of these amazing tailed forms in the cytometric gate corresponding to the GIV.

443 Abundances of GIV could reach 1.1×10^6 VLPs.mL⁻¹ and showed a dynamic with an irregular
444 phase of development (**Fig. 6C**). GIV VLPs were recorded year-round, suggesting that they
445 were dominant with numerous phylotypes and had a potential broad host range. This suggestion
446 was also supported by the correlations between GIV and almost all the microbial compartments
447 (p-value < 0.01).

448 Our data are among the first to document the absolute abundance of this presumably diverse
449 population of *Megaviricetes*. The limited data available to date stemmed from specific isolated
450 and fully described marine phytoplankton viruses during algal bloom^{49–51,61,62}.

451 In the absence of a clear and visible burst event, we used a theoretical BS of 50 to estimate the
452 maximum mortality of 3×10^6 hosts.L⁻¹.day⁻¹ (**Table 1A**).

453

454 *Snake and Sword virus-like particles: New dynamic and specific viruses of microeukaryotes*

455 We report on the discovery of two VLPs above 200 nm, which we called Snake and Sword
456 VLPs on account of their shape (**Fig. 7-8**). One particularity was that they are undetectable by
457 FC based on the measured parameters. This lack of FC detection using dsDNA dye raises the
458 question about the nature of their nucleic acid, probably non-dsDNA. Another explanation is
459 that the signal is hidden within the bulk of VLPs1, VLPs2, or prokaryotes. However, despite
460 their high abundances during the infection period, we found no correlation between TEM counts
461 and any viral cytometric population.

462 Snake VLPs are elongated with a length of 226 nm (**Fig. 7A**). Their neck delimits a spherical
463 part measuring 30 nm in diameter with a cylindrical part of 30 nm in diameter and 100 nm in
464 length and ends with a thinner cylindrical part measuring 15 nm in diameter and 78 nm in
465 length. They have a polarity with a preferential orientation, with the spherical part pointing
466 toward the host (**Fig. 7B**). Snake VLPs infect a flagellated microeukaryote 5 µm in diameter,
467 identified as a heterotrophic Chrysophyceae on morphological and light microscopy criterion⁶³
468 (**Fig. 7B**). These observations were corroborated by the simultaneous dynamics of the
469 abundance of Snake VLPs and Chrysophyceae approximated by 18S metabarcoding data,
470 which were particularly noticeable as Chrysophyceae-dominated eukaryote communities at the
471 time of the Snake VLP bloom (**Fig. 7D**). Snake VLPs were predominant in Lake Chambon,
472 with a maximum abundance of 23.2×10^6 VLPs.mL⁻¹. Their dynamic was characterized by a
473 sudden and massive development strategy with phases of infection alternating with long phases
474 without detection (**Fig. 7C**). The infectivity of Snake VLP was high, with a production capacity
475 exceeding 1,200 VLPs per lysed host. At peak infection, all host cells observed in TEM were
476 infected.

477 Sword VLPs are a head-tail-fiber VLP measuring 635 nm in length (**Fig. 8A**). This viral type
478 is characterized by an elongated dumbbell-shaped head measuring 220 nm in length and
479 between 45 and 135 nm in width, with a sheath-like tail of 370 nm in length and 60 nm in width
480 and fibers distributed at the end of the tail. A thin 9.5 nm thick groove separates the presumed
481 head from the tail. The head has a distinctive substructure resulting from a patterned
482 arrangement of 6 nm diameter subunits. Morphologically, the closest relative appears to be a
483 filamentous VLP previously imaged in a freshwater lake⁶⁴. We reported our observation of
484 infected burst unicellular microeukaryotes of at least 3-4 µm in diameter, but unfortunately, we
485 cannot specify their identity (**Fig. 8B**). Metabarcoding data showed that at time of the VLP
486 bloom, eukaryote communities were dominated by Chrysophyceae (**Fig. 8D**). We found Sword
487 VLP only in Lake SG. Their dynamic, reaching 4.7×10^6 VLPs.mL⁻¹, was characterized by a
488 sudden and massive development strategy (**Fig. 8C**). The BS observed for Sword VLPs
489 appeared to be around 15.

490 On an expanded spatiotemporal scale, we were unable to identify significant correlations (p-
491 value > 0.01) between Snake or Sword VLPs and the autotrophic microbial compartments
492 considered in this study. Nevertheless, focusing on the remarkable viral infection peaks from
493 September 23, 2022, to February 17, 2023, at Lake Chambon and from October 18, 2022, to

494 April 12, 2023, at Lake SG, we showed a clear interaction in the “prey-predator” model between
495 Snake VLPs and heterotrophic flagellated microeukaryotes (**Fig. 7D**) and between Sword VLPs
496 and heterotrophic microeukaryotes or Chrysophyceae, respectively (**Fig. 8D**).

497 The interaction between heterotrophic microeukaryotes, Chrysophyceae, and Sword VLPs was
498 also supported by various observations of numerous Sword VLPs inside a heterotrophic
499 microeukaryotes associated with a putative Chrysophyceae lorica (probably *Dinobryon* sp.) and
500 numerous Sword VLPs around a lorica remnant (**Extended data Fig. 5**).

501 These dynamic analyses support the TEM observations and metabarcoding data showing a
502 putative heterotrophic microeukaryote host for Snake VLPs. The trophic status of the Sword
503 VLP host remains uncertain. Precise identification will require host isolation.

504 Finally, the reproducibility of morphological observations of the Snake and Sword VLPs and
505 their host coupled with their development strategy suggest that they are highly specialist VLPs.

506 These results showed the high involvement of Snake and Sword VLPs in the demise of their
507 host population with a maximum mortality of 0.1 and 2.4×10^7 hosts.L⁻¹.day⁻¹ for Snake and
508 Sword VLPs, respectively (**Table 1A**).

509

510 *Ecological significance of large microeukaryote virus-like particles*

511 This study represents one of the first time series of large microeukaryote VLPs and provides
512 novel insights into their numerical significance in aquatic systems. Detection limitations such
513 as the inability to detect Snake and Sword VLPs using FC will likely lead to an underestimation
514 of the total number of large microeukaryote VLPs. Nevertheless, our data emphasize the
515 numerical importance of these entities in freshwater systems, with total abundances ranging
516 from 0.2 up to 28.4×10^6 VLPs.mL⁻¹. As such, large microeukaryote VLPs accounted for
517 between 0.1 and 2.7%, 0.1 and 6.8%, and 0.3 and 10.8% of the total viral stock in Lakes
518 Fargette, SG, and Chambon, respectively (**Extended data Fig. 6 and Table 1B**). These variable
519 contributions point to the alternating control of microbial systems by large microeukaryote
520 VLPs versus smaller viruses (mostly phages). Of notable interest, this study also reports the
521 significant contribution of large VLPs in an offshore marine site and particularly Shield VLPs,
522 thus expanding the distribution of this morphotype to all aquatic systems.

523 On an annual basis, the productive periods of large VLPs occurred mainly in spring, with some
524 exceptions such as the autumn peak in 2022 in Lake Chambon associated with Snake VLPs and
525 the summer peak in 2022 in Lake Fargette. This strong temporal dynamism was also underlined
526 by the rapid and unexpected successions of specific large VLPs. Some morphotypes (Ham,
527 Shield, Snake, Sword) can evolve from undetectable levels to over 80% of the total large VLPs
528 in a matter of days. At other times, a mixed community of large VLPs was observed in equal
529 proportions (**Extended data Fig. 6A**). Our results were consistent with the “Bank model”⁶⁵,
530 which suggests that only a small fraction of the viral community is active and abundant at any
531 given time, while most populations are rare and dormant, forming a seed bank that can “Kill-
532 the-Winner” when hosts reach critical abundance thresholds⁶⁶. It is worth noting that naked
533 GIV were only dominant once in Lake SG (55% of the total large VLP community on May 30,
534 2022) and that they represent only 12% of all the combined data on average. Thus, large VLPs

535 not previously considered morphologically (Ham, Shield, Snake, Sword) could be prevalent in
536 the microeukaryote ecology of the aquatic environment.

537 To decipher the effect of large microeukaryote VLPs on host communities, we monitored the
538 dynamics of their total abundance concomitantly with those of microbial communities
539 (abundance and diversity). Over the entire study period, the total abundance of large VLPs
540 correlates with the total microeukaryotes ($R^2 = 0.4$, p -value < 0.02). Alongside the observations
541 of “prey-predator” patterns between autotrophic microeukaryotes and Ham VLPs and between
542 heterotrophic microeukaryotes and Snake VLPs (**Fig. 4D, 7D**), these findings suggest that both
543 autotrophic and heterotrophic microeukaryotes contributed significantly and variably to the
544 stock of large VLPs. We observed no significant correlation with abiotic parameters (**Extended**
545 **data Fig. 7**), thus confirming the importance of the microbial environment in the control of
546 large VLPs. The high values of maximum ratios between the total large microeukaryote VLPs
547 and microeukaryotes (325, 949, and 1463 in Lakes Fargette, SG, and Chambon, respectively)
548 (**Table 1B**) point to the significant potential of large VLPs to control microeukaryote
549 populations.

550 We estimated the removal of NMP by large microeukaryote VLPs by calculating the ratio
551 between the theoretical viral-induced mortality of microeukaryotes and net microeukaryote
552 production. NMP removal does not account for viral decay or microeukaryote dynamics during
553 the measurement period, which was limited to a maximum of 2 weeks. It should also be noted
554 that small microeukaryotes (i.e., nanoeukaryotes) are difficult to distinguish from large
555 prokaryotes or fungi spore by light microscopy or FC, and are probably underestimated in
556 microeukaryote counts, which can lead to an overestimation of this ratio. The values ranged
557 from -0.7 to 0.2 in Lake Fargette, from -10 to 37 in Lake SG, and from -6 to 15.6 in Lake
558 Chambon (**Table 1B**). This significant variation indicates that at specific times, large
559 microeukaryote VLPs can control the stock of microeukaryotes and contribute to the observed
560 abundance dynamics (**Extended data Fig. 8**).

561 The potential influence of large VLPs on microeukaryote succession was assessed by analyzing
562 the temporal dynamics of microeukaryotic diversity (Shannon index) in relation to the
563 abundance of large VLPs of microeukaryotes (**Fig. 9**). Our findings showed that episodes of
564 viral production, regardless of the dominant viral type, coincided with a decrease in eukaryote
565 diversity. This pattern is particularly evident in Lake Chambon during the peak of Snake VLPs,
566 which are suspected to control a population of heterotrophic flagellates that prey on other
567 microorganisms⁶⁷. During the massive proliferation of heterotrophic flagellates, which likely
568 causes a drop in diversity, Snake VLPs not only regulate their abundances but also release their
569 predation pressure, which could in turn free up niches for the proliferation of other
570 microeukaryotes. The effects of large VLPs may also be cumulative as in the example of the
571 simultaneous development of Snake VLPs and GIV in Lake Chambon, or they may follow each
572 other successively as in the example of the successive production of Ham and Shield VLPs in
573 Lake Fargette. Although it is clear that large VLP communities were an essential factor in
574 regulating the succession of microeukaryote communities in our study sites, the lack of
575 information regarding their life traits (e.g., infection mode, host specificities) or subcellular
576 interactions limits our understanding of their overall impact. Dedicated efforts to isolate and
577 characterize the interactions of large VLPs must be pursued in order to gain insights into the
578 role of this underexplored, yet significant component of the virosphere by means of cultures,
579 subcellular observations, and transcriptomic analyses^{3,25,68}.

580 Surprisingly, the minimum values for the abundance, microeukaryotic virus/total virus ratio,
581 microeukaryote VLP and microeukaryote ratio, and NMP removal by large microeukaryotic
582 VLPs were encountered in Lake Fargette, which presents the highest microbial abundances and
583 pigment contents (**Table 1, Extended Data Fig. 6 and 8**), thus suggesting better control in less
584 eutrophic environments.

585

586 **Conclusions and perspectives**

587 At a large temporal scale, the combination of FC and TEM led to original and unexpected
588 advances in determining the diversity and ecology of large aquatic VLPs. Indeed, we shed light
589 on the astonishing phenotypic diversity of large VLPs in aquatic ecosystems, with the
590 identification of specific cytometric populations and four novel morphotypes never previously
591 described. These viruses, which infect prokaryotes or microeukaryotes undoubtedly play a role
592 in the control of their host population. Each type of VLP probably represents different
593 taxonomic levels and specializations (from specialist to generalist). Some notably seem to infect
594 heterotrophic microeukaryotes, for which few viruses have been reported. The global
595 community of large VLPs, considered here for the first time on a large temporal scale, showed
596 marked dynamics in terms of both their abundance and diversity, with each of the studied types
597 either succeeding or accumulating. We suggest that these viral communities have a very strong
598 impact on ecosystem functioning by controlling the dynamics of prokaryotic and eukaryotic
599 communities, both autotrophic and heterotrophic, and by controlling their diversity, which
600 implies their major role, hitherto unimagined at such a scale, in the functioning of the
601 ecosystem.

602 These discoveries significantly impact our perception of the virosphere, its diversity, and the
603 role played by large viruses in the dynamism of their hosts and the functioning of aquatic food
604 webs. This study urges us to investigate the genomic characterization of these VLPs and to
605 identify their host to fully explore these concepts. Advances in metatranscriptomic technologies
606 will allow us to better clarify their role in the matter and energy flow of ecosystems by gaining
607 access to their cellular and subcellular levels.

608

609 **Data availability**

610 Relevant data supporting the key findings of this study are available in the article and the
611 Supplementary Information file. All raw data generated du the current study are available from
612 the corresponding author upon request.

613

614

615 **References**

- 616 1. Rohwer, F. & Thurber, R. V. Viruses manipulate the marine environment. *Nature* **459**, 207–212
617 (2009).
- 618 2. Weinheimer, A. R. & Aylward, F. O. Infection strategy and biogeography distinguish
619 cosmopolitan groups of marine jumbo bacteriophages. *The ISME Journal* **16**, 1657–1667 (2022).
- 620 3. Hevroni, G., Vincent, F., Ku, C., Sheyn, U. & Vardi, A. Daily turnover of active giant virus
621 infection during algal blooms revealed by single-cell transcriptomics. *Sci. Adv.* **9**, eadf7971
622 (2023).
- 623 4. Vincent, F. *et al.* Viral infection switches the balance between bacterial and eukaryotic recyclers
624 of organic matter during coccolithophore blooms. *Nat Commun* **14**, 510 (2023).
- 625 5. Van Etten, J. L., Burbank, D. E., Kuczmarski, D. & Meints, R. H. Virus Infection of Culturable
626 *Chlorella* -Like Algae and Development of a Plaque Assay. *Science* **219**, 994–996 (1983).
- 627 6. Krylov, V. N. & Zhazykov, I. Z. [Pseudomonas bacteriophage phiKZ--possible model for
628 studying the genetic control of morphogenesis]. *Genetika* **14**, 678–685 (1978).
- 629 7. Van Etten, J. L. & Meints, R. H. Giant Viruses Infecting Algae. *Annu. Rev. Microbiol.* **53**, 447–
630 494 (1999).
- 631 8. Scola, B. L. *et al.* A Giant Virus in Amoebae. *Science* **299**, 2033–2033 (2003).
- 632 9. Pagnier, I. *et al.* A Decade of Improvements in Mimiviridae and Marseilleviridae Isolation from
633 Amoeba. *Intervirology* **56**, 354–363 (2013).
- 634 10. Claverie, J.-M. & Abergel, C. Mimiviridae: An Expanding Family of Highly Diverse Large
635 dsDNA Viruses Infecting a Wide Phylogenetic Range of Aquatic Eukaryotes. *Viruses* **10**, 506
636 (2018).
- 637 11. Yuan, Y. & Gao, M. Jumbo Bacteriophages: An Overview. *Front. Microbiol.* **8**, (2017).
- 638 12. Coy, S., Gann, E., Pound, H., Short, S. & Wilhelm, S. Viruses of Eukaryotic Algae: Diversity,
639 Methods for Detection, and Future Directions. *Viruses* **10**, 487 (2018).
- 640 13. Keeling, P. J. & Campo, J. del. Marine Protists Are Not Just Big Bacteria. *Current Biology* **27**,
641 R541–R549 (2017).

- 642 14. Schulz, F. *et al.* Giant virus diversity and host interactions through global metagenomics. *Nature*
643 **578**, 432–436 (2020).
- 644 15. Endo, H. *et al.* Biogeography of marine giant viruses reveals their interplay with eukaryotes and
645 ecological functions. *Nat Ecol Evol* **4**, 1639–1649 (2020).
- 646 16. Al-Shayeb, B. *et al.* Clades of huge phages from across Earth’s ecosystems. *Nature* **578**, 425–431
647 (2020).
- 648 17. Ha, A. D., Moniruzzaman, M. & Aylward, F. O. Assessing the biogeography of marine giant
649 viruses in four oceanic transects. *ISME Communications* **3**, 43 (2023).
- 650 18. Zhang, L., Meng, L., Fang, Y., Ogata, H. & Okazaki, Y. Spatiotemporal dynamics revealed the
651 dark water community of giant virus from a deep freshwater lake. Preprint at
652 <https://doi.org/10.1101/2024.04.21.590434> (2024).
- 653 19. Koonin, E. V. *et al.* Global Organization and Proposed Megataxonomy of the Virus World.
654 *Microbiol Mol Biol Rev* **84**, e00061-19 (2020).
- 655 20. Aylward, F. O., Moniruzzaman, M., Ha, A. D. & Koonin, E. V. A phylogenomic framework for
656 charting the diversity and evolution of giant viruses. *PLoS Biol* **19**, e3001430 (2021).
- 657 21. Abergel, C., Legendre, M. & Claverie, J.-M. The rapidly expanding universe of giant viruses:
658 Mimivirus, Pandoravirus, Pithovirus and Mollivirus. *FEMS Microbiology Reviews* **39**, 779–796
659 (2015).
- 660 22. M. Iyer, L., Anantharaman, V., Krishnan, A., Burroughs, A. M. & Aravind, L. Jumbo Phages: A
661 Comparative Genomic Overview of Core Functions and Adaptions for Biological Conflicts.
662 *Viruses* **13**, 63 (2021).
- 663 23. Gaïa, M. & Forterre, P. From Mimivirus to Mirusvirus: The Quest for Hidden Giants. *Viruses* **15**,
664 1758 (2023).
- 665 24. Gaïa, M. *et al.* Mirusviruses link herpesviruses to giant viruses. *Nature* **616**, 783–789 (2023).
- 666 25. Fromm, A. *et al.* Single-cell RNA-seq of the rare virosphere reveals the native hosts of giant
667 viruses in the marine environment. *Nat Microbiol* (2024) doi:10.1038/s41564-024-01669-y.
- 668 26. Fischer, M. G., Mersdorf, U. & Blanchard, J. L. Amazing structural diversity of giant virus-like
669 particles in forest soil. Preprint at <https://doi.org/10.1101/2023.06.30.546935> (2023).

- 670 27. Brussaard, C. P. D., Thyrraug, R., Marie, D. & Bratbak, G. FLOW CYTOMETRIC ANALYSES
671 OF VIRAL INFECTION IN TWO MARINE PHYTOPLANKTON SPECIES, *MICROMONAS*
672 *PUSILLA* (PRASINOPHYCEAE) AND *PHAEOCYSTIS POUCHETII*
673 (PRYMNESIOPHYCEAE). *Journal of Phycology* **35**, 941–948 (1999).
- 674 28. Jacquet, S. *et al.* Flow cytometric analysis of an *Emiliana huxleyi* bloom terminated by viral
675 infection. *Aquat. Microb. Ecol.* **27**, 111–124 (2002).
- 676 29. Brussaard, C. P. D. Optimization of Procedures for Counting Viruses by Flow Cytometry. *Appl*
677 *Environ Microbiol* **70**, 1506–1513 (2004).
- 678 30. Baudoux, A., Noordeloos, A., Veldhuis, M. & Brussaard, C. Virally induced mortality of
679 *Phaeocystis globosa* during two spring blooms in temperate coastal waters. *Aquat. Microb. Ecol.*
680 **44**, 207–217 (2006).
- 681 31. Larsen, J. B., Larsen, A., Thyrraug, R., Bratbak, G. & Sandaa, R.-A. Response of marine viral
682 populations to a nutrient induced phytoplankton bloom at different pCO₂ levels. *Biogeosciences* **5**, 523–533 (2008).
- 683 32. Personnic, S., Domaizon, I., Dorigo, U., Berdjeb, L. & Jacquet, S. Seasonal and spatial variability
684 of virio-, bacterio-, and picophytoplanktonic abundances in three peri-alpine lakes. *Hydrobiologia*
685 **627**, 99–116 (2009).
- 686 33. Biggs, T. E. G., Huisman, J. & Brussaard, C. P. D. Viral lysis modifies seasonal phytoplankton
687 dynamics and carbon flow in the Southern Ocean. *The ISME Journal* **15**, 3615–3622 (2021).
- 688 34. Khalil, J. Y. B. *et al.* Flow Cytometry Sorting to Separate Viable Giant Viruses from Amoeba Co-
689 culture Supernatants. *Front. Cell. Infect. Microbiol.* **6**, (2017).
- 690 35. Martínez, J. M., Swan, B. K. & Wilson, W. H. Marine viruses, a genetic reservoir revealed by
691 targeted viromics. *The ISME Journal* **8**, 1079–1088 (2014).
- 692 36. Martinez-Hernandez, F. *et al.* Single-virus genomics reveals hidden cosmopolitan and abundant
693 viruses. *Nat Commun* **8**, 15892 (2017).
- 694 37. De Corte, D. *et al.* Viral Communities in the Global Deep Ocean Conveyor Belt Assessed by
695 Targeted Viromics. *Front. Microbiol.* **10**, 1801 (2019).
- 696

- 697 38. Martínez Martínez, J., Martínez-Hernandez, F. & Martínez-García, M. Single-virus genomics and
698 beyond. *Nat Rev Microbiol* **18**, 705–716 (2020).
- 699 39. Mojica, K. D. A., Huisman, J., Wilhelm, S. W. & Brussaard, C. P. D. Latitudinal variation in
700 virus-induced mortality of phytoplankton across the North Atlantic Ocean. *The ISME Journal* **10**,
701 500–513 (2016).
- 702 40. Brussaard, Corina PD and Martinez, J Martinez. Algal bloom viruses. *Plant Viruses* **2**, 1–13
703 (2008).
- 704 41. Brussaard, C. P. D., Payet, J. P., Winter, C. & Weinbauer, M. G. Quantification of aquatic viruses
705 by flow cytometry. in *Manual of Aquatic Viral Ecology* (eds. Wilhelm, S., Weinbauer, M. &
706 Suttle, C.) 102–109 (American Society of Limnology and Oceanography, 2010).
707 doi:10.4319/mave.2010.978-0-9845591-0-7.102.
- 708 42. Lawrence, J. E., Brussaard, C. P. D. & Suttle, C. A. Virus-Specific Responses of *Heterosigma*
709 *akashii* to Infection. *Appl Environ Microbiol* **72**, 7829–7834 (2006).
- 710 43. Tomaru, Y. & Nagasaki, K. Flow cytometric detection and enumeration of DNA and RNA viruses
711 infecting marine eukaryotic microalgae. *J Oceanogr* **63**, 215–221 (2007).
- 712 44. Baudoux, A.-C. & Brussaard, C. P. D. Characterization of different viruses infecting the marine
713 harmful algal bloom species *Phaeocystis globosa*. *Virology* **341**, 80–90 (2005).
- 714 45. Rasband, W.S. *ImageJ*, U. S. (<https://imagej.net/ij/>, National Institutes of Health, Bethesda,
715 Maryland, USA).
- 716 46. Nazir, A., Ali, A., Qing, H. & Tong, Y. Emerging Aspects of Jumbo Bacteriophages. *IDR*
717 **Volume 14**, 5041–5055 (2021).
- 718 47. Hu, M. *et al.* Characterization of a novel genus of jumbo phages and their application in
719 wastewater treatment. *iScience* **26**, 106947 (2023).
- 720 48. Shinn, G. L. & Bullard, B. L. Ultrastructure of Meelsvirus: A nuclear virus of arrow worms
721 (phylum Chaetognatha) producing giant “tailed” virions. *PLoS ONE* **13**, e0203282 (2018).
- 722 49. Tarutani, K., Nagasaki, K. & Yamaguchi, M. Viral Impacts on Total Abundance and Clonal
723 Composition of the Harmful Bloom-Forming Phytoplankton *Heterosigma akashiwo*. *Appl*
724 *Environ Microbiol* **66**, 4916–4920 (2000).

- 725 50. Sorensen, G., Baker, A. C., Hall, M. J., Munn, C. B. & Schroeder, D. C. Novel virus dynamics in
726 an *Emiliana huxleyi* bloom. *Journal of Plankton Research* **31**, 787–791 (2009).
- 727 51. Bellec, L., Grimsley, N., Derelle, E., Moreau, H. & Desdevises, Y. Abundance, spatial
728 distribution and genetic diversity of *Ostreococcus tauri* viruses in two different environments.
729 *Environ Microbiol Rep* **2**, 313–321 (2010).
- 730 52. Baudoux, A. -C. *et al.* Interplay between the genetic clades of *M. icromonas* and their viruses in
731 the Western English Channel. *Environ Microbiol Rep* **7**, 765–773 (2015).
- 732 53. Vieira, H. H. *et al.* Isolation of a widespread giant virus implicated in cryptophyte bloom collapse.
733 *The ISME Journal* **18**, wrac029 (2024).
- 734 54. Deeg, C. M., Chow, C.-E. T. & Suttle, C. A. The kinetoplastid-infecting Bodo saltans virus (BsV),
735 a window into the most abundant giant viruses in the sea. *eLife* **7**, e33014 (2018).
- 736 55. Alempic, J.-M. *et al.* An Update on Eukaryotic Viruses Revived from Ancient Permafrost. *Viruses*
737 **15**, 564 (2023).
- 738 56. Notaro, A. *et al.* Expanding the Occurrence of Polysaccharides to the Viral World: The Case of
739 Mimivirus. *Angew Chem Int Ed* **60**, 19897–19904 (2021).
- 740 57. Takahashi, H., Fukaya, S., Song, C., Murata, K. & Takemura, M. Morphological and Taxonomic
741 Properties of the Newly Isolated *Cotonvirus japonicus*, a New Lineage of the Subfamily
742 *Megavirinae*. *J Virol* **95**, e00919-21 (2021).
- 743 58. Garza, D. & Suttle, C. Large double-stranded DNA viruses which cause the lysis of a marine
744 heterotrophic nanoflagellate (*Bodo* sp.) occur in natural marine viral communities. *Aquat. Microb.*
745 *Ecol.* **9**, 203–210 (1995).
- 746 59. Schulz, F. *et al.* Giant viruses with an expanded complement of translation system components.
747 *Science* **356**, 82–85 (2017).
- 748 60. Sun, T.-W. *et al.* Host Range and Coding Potential of Eukaryotic Giant Viruses. *Viruses* **12**, 1337
749 (2020).
- 750 61. Wilson, W. H., Van Etten, J. L. & Allen, M. J. The Phycodnaviridae: The Story of How Tiny
751 Giants Rule the World. in *Lesser Known Large dsDNA Viruses* (ed. Van Etten, J. L.) vol. 328 1–
752 42 (Springer Berlin Heidelberg, Berlin, Heidelberg, 2009).

- 753 62. Lehahn, Y. *et al.* Decoupling Physical from Biological Processes to Assess the Impact of Viruses
754 on a Mesoscale Algal Bloom. *Current Biology* **24**, 2041–2046 (2014).
- 755 63. Jeuck, A. & Arndt, H. A Short Guide to Common Heterotrophic Flagellates of Freshwater
756 Habitats Based on the Morphology of Living Organisms. *Protist* **164**, 842–860 (2013).
- 757 64. Hofer, J. & Sommaruga, R. Seasonal dynamics of viruses in an alpine lake: importance of
758 filamentous forms. *Aquatic microbial ecology*. **26**, (2001).
- 759 65. Breitbart, M. & Rohwer, F. Here a virus, there a virus, everywhere the same virus? *Trends in*
760 *Microbiology* **13**, 278–284 (2005).
- 761 66. Thingstad, T. F. Elements of a theory for the mechanisms controlling abundance, diversity, and
762 biogeochemical role of lytic bacterial viruses in aquatic systems. *Limnology & Oceanography* **45**,
763 1320–1328 (2000).
- 764 67. Jeong, M., Kim, J. I., Nam, S. W. & Shin, W. Molecular Phylogeny and Taxonomy of the Genus
765 *Spumella* (Chrysophyceae) Based on Morphological and Molecular Evidence. *Front. Plant Sci.*
766 **12**, 758067 (2021).
- 767 68. Wang, J., Li, L. & Lin, S. Active viral infection during blooms of a dinoflagellate indicates
768 dinoflagellate-viral co-adaptation. *Appl Environ Microbiol* **89**, e01156-23 (2023).

769

770 **Acknowledgements**

771 This project received financial support from the CNRS through the MITI interdisciplinary
772 programs (X-life 2018-2019, Origines 2020-2021, and PIB 2023-2024). We also benefited from
773 the following: (i) the CPER 2015–2020 SYMBIOSE challenge program (French Ministry of
774 Research, UCA, CNRS, INRA, Auvergne-Rhone-Alpes Region, FEDER), which supported the
775 PhD fellowship of M.F.; (ii) funding from the French government IDEX-ISITE initiative 16-
776 IDEX- 0001 (CAP 20–25); and (iii) the contribution of the APERO project funded by the
777 National Research Agency under the grant APERO [grant number ANR ANR-21-CE01-0027]
778 and by the French LEFE-Cyber program (CNRS, INSU). We would also like to thank the
779 SYSTEM–UCA PARTNER Platform (Clermont-Ferrand, FRANCE) for their technical
780 support and expertise.

781 We are grateful to Dr Mart Krupovic for his expertise and numerous discussions and for his
782 help in drafting the manuscript.

783 We are indebted to all those who contributed to these efforts.

784

785 **Author information**

786 Authors and Affiliations

787 **Laboratoire Microorganismes : Génome et Environnement (LMGE), UMR CNRS 6023,**
788 **Université Clermont-Auvergne, F-63000 Clermont-Ferrand, France**

789

790 Hermine Billard, Maxime Fuster, François Enault, Jean-François Carrias, Léa Fargette,
791 Margot Carrouée, Perrine Desmares, Téléphore Sime-Ngando, Jonathan Colombet

792 **Génomique Métabolique, Genoscope, Institut François Jacob, CEA, CNRS, Univ. Evry,**
793 **Université Paris-Saclay, Evry, France**

794 Tom O. Delmont

795 **Sorbonne Université, CNRS, Station Biologique de Roscoff, FR2424, Roscoff, France**

796 Gwenn Tanguy

797 **Sorbonne Université, CNRS, Station Biologique de Roscoff, UMR 7144, Roscoff, France**

798 Estelle Bigeard, Pauline Nogaret, Anne-Claire Baudoux

799 **UMR CNRS 8187 LOG, Université Littoral Côte d'Opale, Université de Lille,**
800 **Wimereux, France**

801 Urania Christaki

802

803 **Contributions**

804 J.C. supervised this research. H.B. and J.C. conceived the project, designed and led the
805 experiment. E.B., G.T., P.N., A.C.B., and U.C. provided the marine samples. H.B. and J.C. co-
806 wrote the manuscript. J.F.C., H.B., and P.D. analyzed the diversity of the microeukaryotes. All
807 authors contributed to the data analysis and discussion.

808 *Corresponding author

809 Correspondence to Jonathan Colombet: jonathan.colombet@uca.fr

810

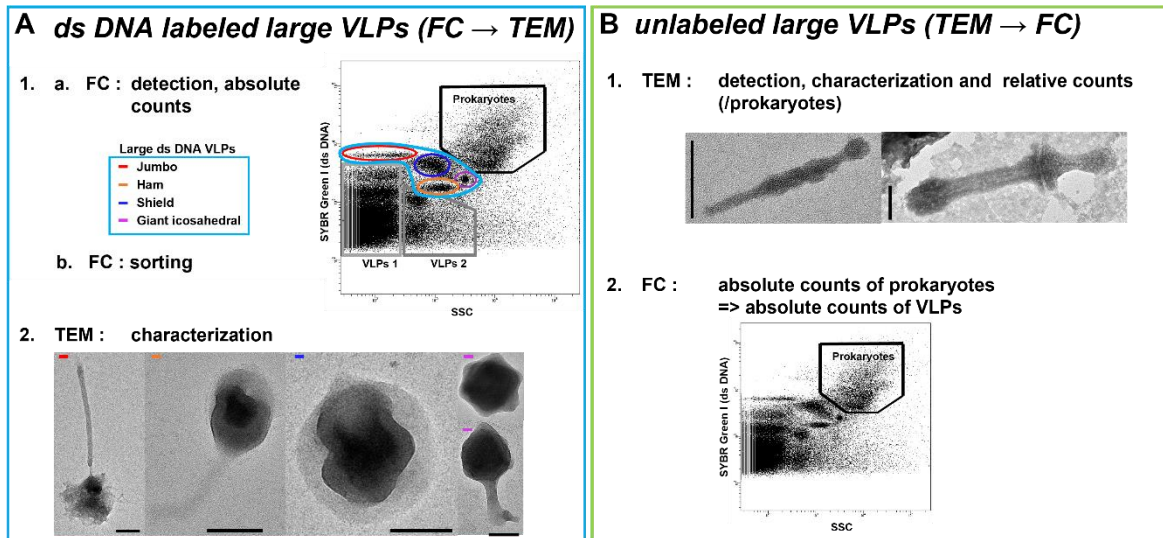
811 **Ethical declarations**

812 Competing interests

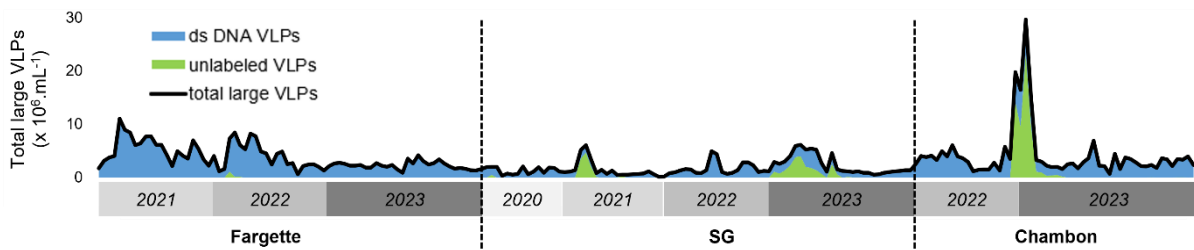
813 The authors declare no competing interests.

814

1 Figures



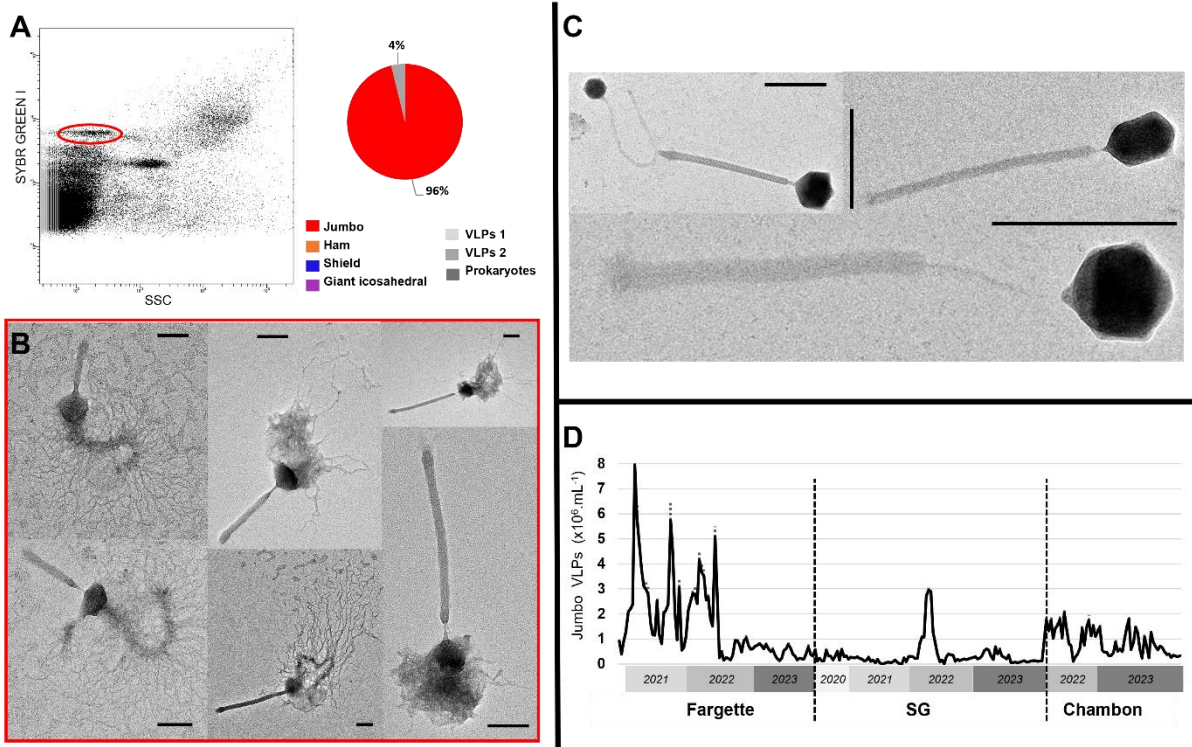
2
3 **Fig. 1** Workflow of the methodological strategy of coupling flow cytometry (FC) /
4 transmission electron microscopy (TEM) to detect, characterize and count large virus-like
5 particles (VLPs) ds DNA labeled (A) and unlabeled (B). **A1**, Dot plot of the gating strategy
6 for the analysis of viral and microbial communities used in the temporal survey with emphasis
7 on large dsDNA-labeled VLPs determined according to their ds DNA content (SYBR Green
8 I) and side scatter (SSC) intensities. 8 populations were considered: Jumbo, Shield, Ham,
9 giant icosahedral VLPs (the sum of these VLPs constitutes the large dsDNA VLPs), VLPs 1
10 and 2 and prokaryotes. **A2**, Negative staining electron micrographs micrographs of large
11 dsDNA-specific VLPs sorted by FC into FC-identified gates. **B1**, Negative staining electron
12 micrographs of large unlabeled specific VLPs detected in environmental samples. **B2**, Dot
13 plot of the gating strategy for the analysis of prokaryotes used to convert relative counts of
14 unlabeled large VLPs into absolute counts. Scale bars = 100 nm.



18
19 **Fig. 2** Seasonal dynamics of the abundance of total community of large virus-like particles
20 (VLPs) (labeled and unlabeled), in lakes Fargette, SG and Chambon. Each data represents the
21 average of triplicates, n= 209.

22
23

24

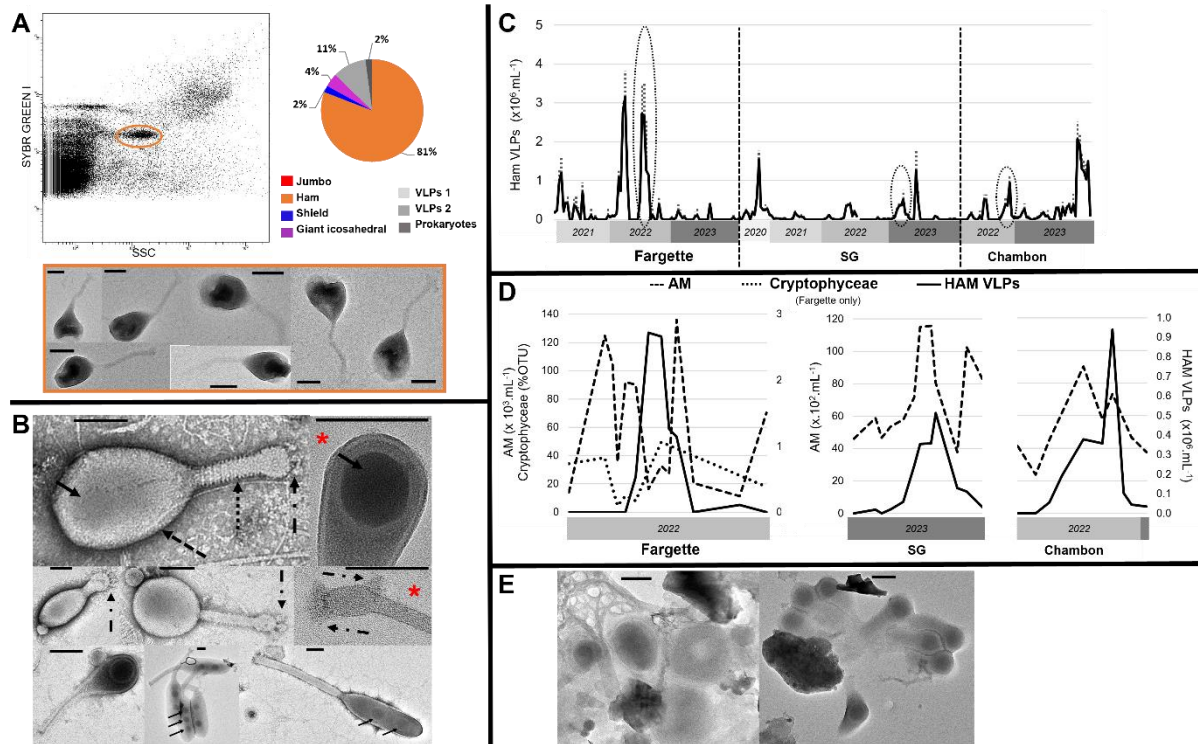


25

26 **Fig. 3** Detection, morphological and ecological characterization of Jumbo-like phage
27 populations identified in eutrophic French lakes. **A**, Flow cytometry (FC) detection of a Jumbo-
28 like phage population and diversity of entities recorded by transmission electron microscopy of
29 this sorted population. **B**, Negative staining electron micrographs displayed Jumbo-like phages
30 obtained in the sorted population. Note the deleterious effect of sorting with visible damage on
31 the capsid of Jumbo-like phages on which the molecular structure comes out of the head. **C**,
32 Negative staining electron micrographs of Jumbo-like phages detected in environmental
33 samples. Scale bars in B = 100 nm, C = 200 nm. **D**, Seasonal dynamics of Jumbo-like phage
34 abundances, in lakes Fargette, SG and Chambon. Each data represents the average of triplicates,
35 dotted lines indicate standard deviation. n = 252.

36

37

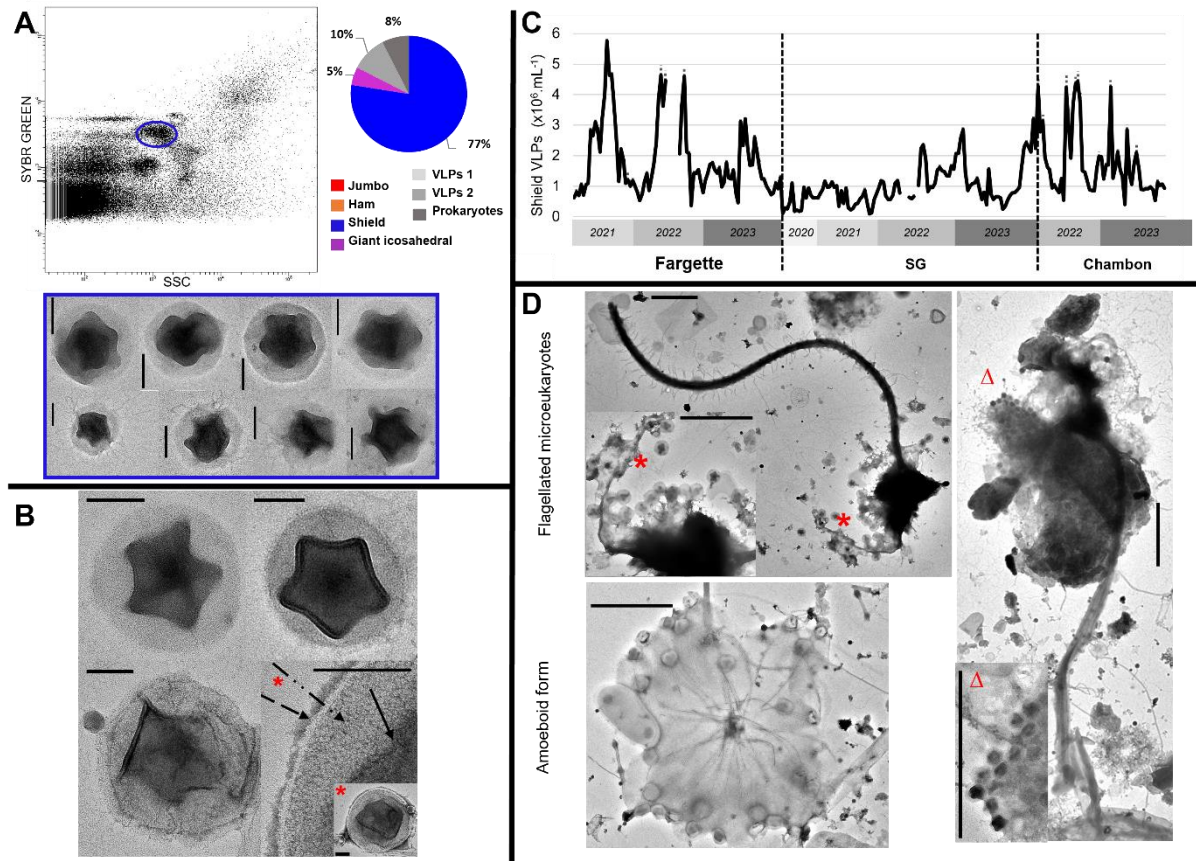


38

39 **Fig. 4** Detection, morphological and ecological characterization of Ham virus-like particles
 40 (VLPs) detected in eutrophic French lakes. **A**, Flow cytometry (FC) detection of remarkable
 41 population of Ham VLPs and diversity of entities recorded by transmission electron microscopy
 42 after FC sorting in the corresponding population with micrographs of the Ham VLPs sorted.
 43 Note the deleterious effect of sorting with visible damage on the capsid of Ham VLPs. **B**,
 44 Negative staining electron micrographs of Ham VLPs in which we detected an, two or three
 45 icosahedral structures (\rightarrow) contained within a surrounding structure with a head (\dashrightarrow)-tail (
 46 $\cdots\rightarrow$) morphology. * Illustrated zoom on head or tail. Note the spiral-shaped molecular structure
 47 around the tail ($\cdots\rightarrow$) and the presence of fibers (\dashrightarrow) at the end of the tail. **C**, Seasonal
 48 dynamics of the abundance of Ham VLPs, in lakes Fargette, SG and Chambon. Each data
 49 represents the average of triplicates, dotted lines indicate standard deviation. $n=252$. **D**, Focus
 50 on remarkable infection periods on the covariations of Ham VLPs and autotrophic
 51 microeukaryotes (AM) and relative abundance of Cryptophyceae class (% OTU) in lake
 52 Fargette from March 29, 2022 to August 30, 2022, in lake SG from January 16, 2023 to April
 53 12, 2023, and in lake Chambon from September 23, 2022 to January 3, 2023. **E**, Negative
 54 staining electron micrographs of Ham VLPs derived from a lytic event. Scale bars A, B, E =
 55 100 nm.

56

57

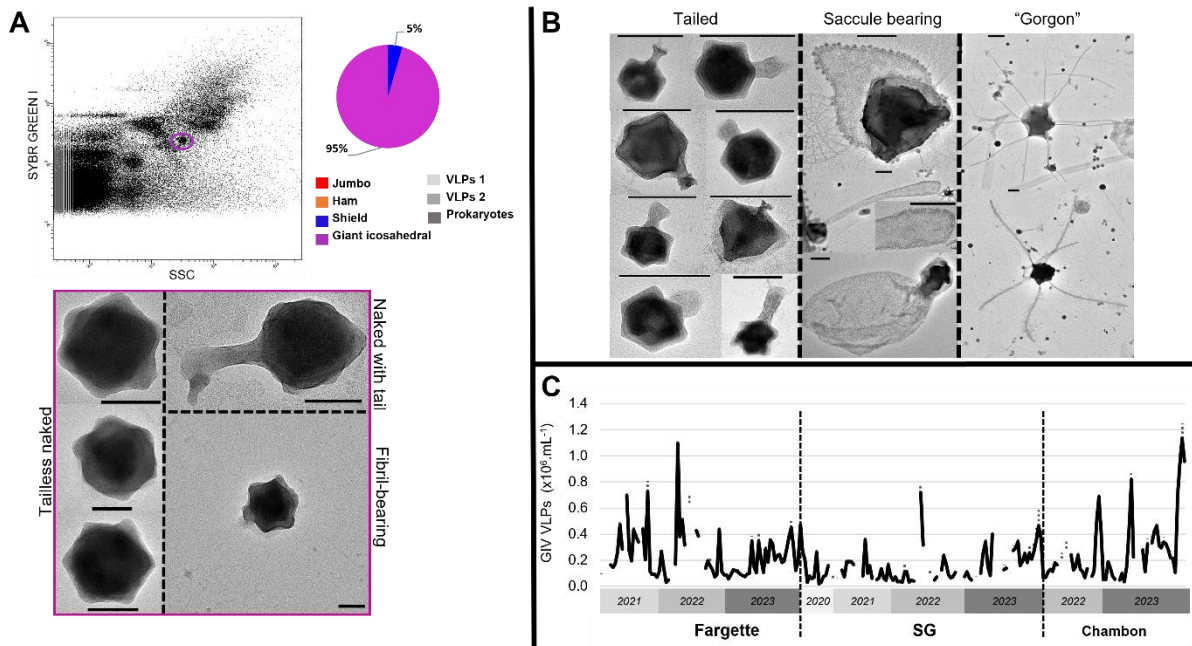


58

59 **Fig. 5** Detection, morphological and ecological characterization of Shield virus-like particle
 60 (VLPs) detected in eutrophic French lakes. **A**, Flow cytometry (FC) detection of remarkable
 61 population of Shield VLPs and diversity of entities recorded by transmission electron
 62 microscopy after FC sorting in the corresponding population with negative staining electron
 63 micrographs of the Shield VLPs sorted. **B**, Negative staining electron micrographs of Shield
 64 VLPs in which we identified an inner pentagonal structure (→) surrounded by a tegument (→→)
 65 and an envelope (←→)-like structure. Note the stargate-like motif in the center of the
 66 inner structure. **C**, Seasonal dynamics of the abundance of Shield VLPs, in lakes Fargette, SG
 67 and Chambon. Each data represents the average of triplicates, dotted lines indicate standard
 68 deviation. n=243. **D**, Negative staining electron micrographs of Shield VLPs derived from lytic
 69 events of flagellated microeukaryotes or amoeboid form hosts. Scale bars A, B = 100 nm, D =
 70 1 μm. *ΔIllustrated zoom parts.

71

72



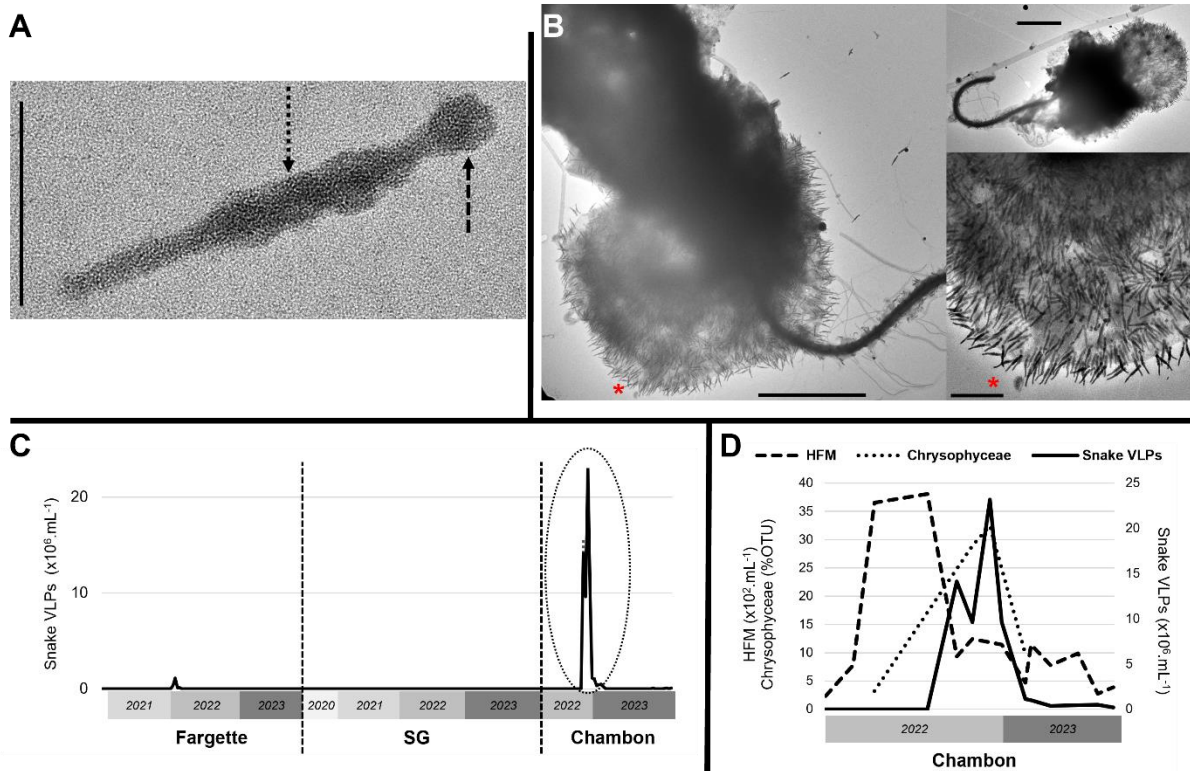
73

74 **Fig. 6** Detection, morphological and ecological characterization of giant icosahedral virus-like
 75 particles (GIV) detected in eutrophic French lakes. **A**, Flow cytometry (FC) detection of
 76 remarkable population of GIV and diversity of entities recorded by transmission electron
 77 microscopy after FC sorting in the corresponding population with micrographs of the GIV
 78 sorted. **B**, Negative staining electron micrographs of various GIV, tailed, bearing a saccule or
 79 "Gorgon". Scale bars A = 100 nm, B = 200 nm. **C**, Seasonal dynamics of the abundance of
 80 GIV, in lakes Fargette, SG and Chambon. Each data represents the average of triplicates, dotted
 81 lines indicate standard deviation. n=209.

82

83

84

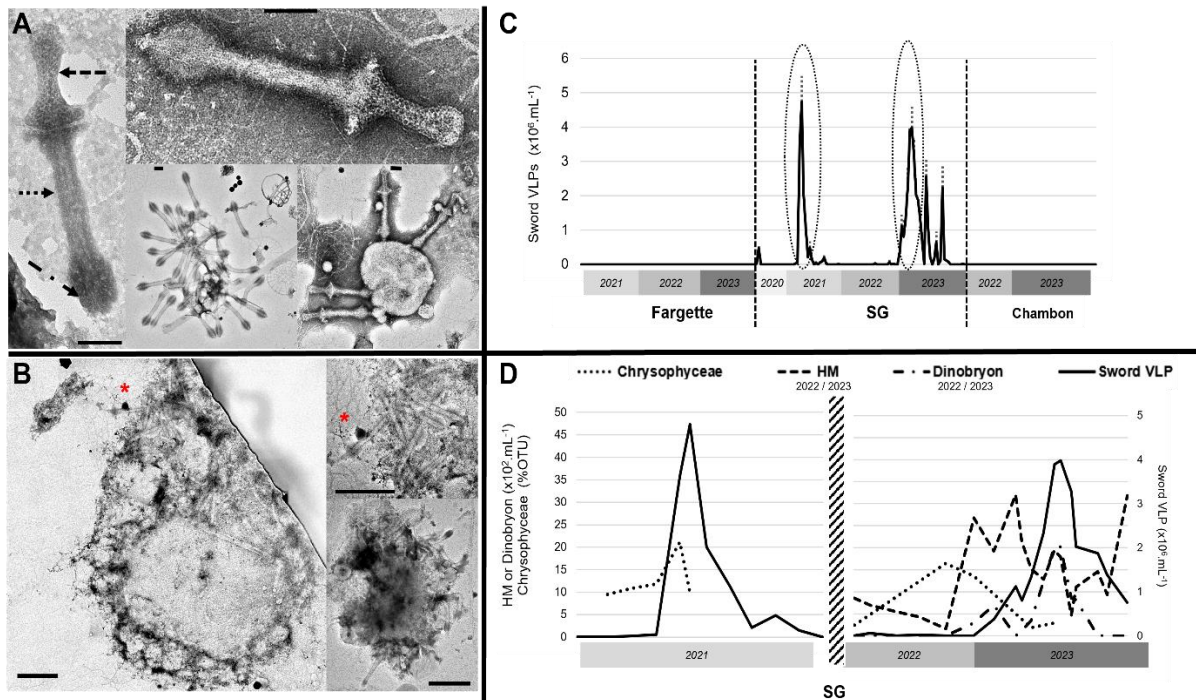


85

86 **Fig. 7** Detection, morphological and ecological characterization of Snake virus-like particles
87 (VLPs) detected in eutrophic French lakes. **A**, Negative staining electron micrographs of
88 Snake VLP showing two prominent parts (--->) and (.....>). **B**, Negative staining electron
89 micrographs of Snake VLPs derived from a lytic event in a microeukaryote host. * Illustrated
90 zoom part. **C**, Seasonal dynamics of the abundance of Snake VLPs, in lakes Fargette, SG and
91 Chambon. Each data represents the average of triplicates, dotted lines indicate standard
92 deviation. n=252. Scale bars A = 200 nm, B = 2 μ m with scale in zoom part = 500 nm. **D**,
93 Focus on remarkable infection periods on the dynamics of Snake VLPs, heterotrophic
94 flagellated microeukaryotes (HFM) and relative abundance of Chrysophyceae class (% OTU)
95 in lake Chambon from September 23, 2022 to February 17, 2023.

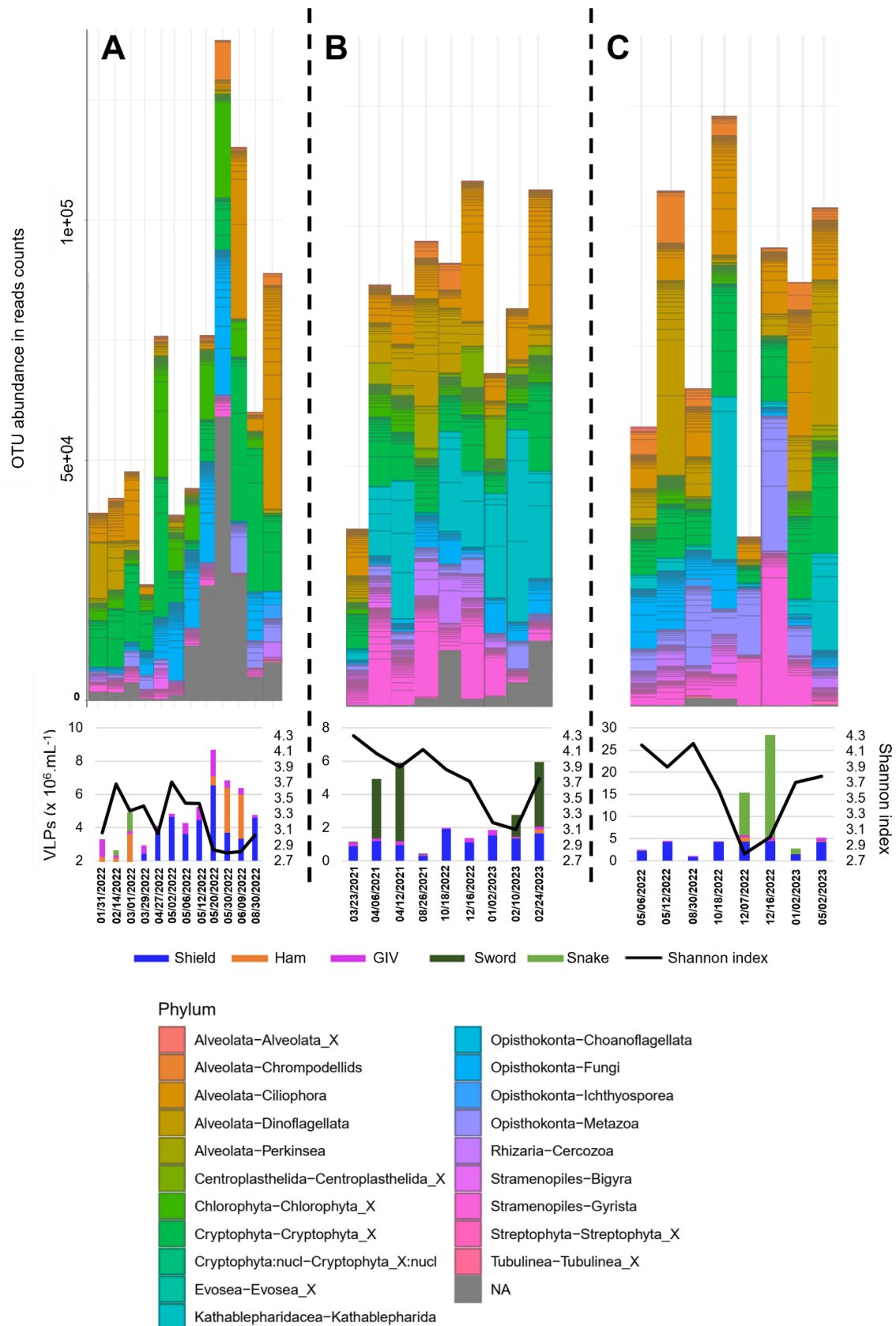
96

97



98

99 **Fig. 8** Detection, morphological and ecological characterization of Sword virus-like particles
 100 (VLPs) detected in eutrophic French lakes. **A**, Negative staining electron micrographs of
 101 Sword VLPs with a head (---) -tail (····) morphology terminated by fibers (—··). **B**,
 102 Negative staining electron micrographs of Sword VLPs derived from a lytic event in a
 103 microeukaryote host. * Illustrated zoom part. Scale bars A = 100 nm, B = 500 nm. **C**,
 104 Seasonal dynamics of the abundance of Sword VLPs, in lakes Fargette, SG and Chambon.
 105 Each data represents the average of triplicates, dotted lines indicate standard deviation. n=252.
 106 **D**, Focus on remarkable infection periods on the covariations of sword VLPs, heterotrophic
 107 microeukaryotes (HM) and Dinobryon sp., and relative abundance of Chrysophyceae classes
 108 (% OTU) in lake SG from February 04, 2021 to June 30, 2021 and from October 18, 2022 to
 109 April 12, 2023.



110

111 **Fig. 9** Temporal dynamics of eukaryote OTU abundance in reads counts, and of eukaryote
 112 diversity index (Shannon index) compare to viral abundance of Ham, Shield, Snake, Sword
 113 and giant icosahedral viruses (GIV) in lakes Fargette (A), SG (B) and Chambon (C).

A

Type	Size (nm)	VLPs abundance (min-max) x10 ⁸ ·mL ⁻¹	Plausible host	Burst Size (BS)	NVP max (x10 ⁸ viruses.L ⁻¹ .day ⁻¹)	VDRM max (x10 ⁷ hosts.L ⁻¹ day ⁻¹)
Shield	194-460 (virion) icosahedra 140-300	0.3 - 13.7	Various microeukaryotes	27	3.6	1.3
Ham	Pleomorphic 450-1070 (head-tail), icosahedra 75-80	ND - 3.1	Cryptophyceae	8	2.3	2.9
Snake	226 length	ND - 23.2	Heterotrophic Chrysophyceae	≈ 1 200	15.1	0.1
Sword	635 (head-tail)	ND - 4.7	Microeukaryotes	15	3.6	2.4
Giant Icosahedral	Pleomorphic 180-230 (untail), 360 (head-tail)	0.02 - 1.1	Microeukaryotes	(theoretical) 50	1.6	0.3
Jumbo	300-600 (head-tail), icosahedra 90-120	0.002-7.9	Prokaryotes	(theoretical) 50	5.9	1.1

BS Burst Size

NVP Net large microeuk. VLPs Production = $[VLPs (time N) - VLPs (time N-1)] / Elapsed\ time$

VDRM theoretical Viral Death Rate of Microeuk. = NVP/BS

MVMR Large Microeuk. VLPs to Microeuk. Ratio = $Large\ microeuk.\ VLPs\ abundance / Microeuk.\ abundance$

MVTVR Large Microeuk. VLPs to Total VLPs Ratio = $Large\ microeuk.\ VLP\ abundance / Total\ VLPs\ abundance$

NMP Net Microeukaryotes Production = $[Microeuk.\ (time\ N) - Microeuk.\ (time\ N-1)] / Elapsed\ time$

Removal of NMP = $VDRM/NMP$

B

Lake	MVMR (min-max)	MVTVR (%)	Removal of NMP (min-max)
Fargette	2-325	0.1 - 2.7	-0.7 - 0.2
SG	1-949	0.1 - 6.8	-10 - 37
Chambon	11-1463	0.3 - 10.8	-6 - 15.6

114

115 **Table 1** Morphological and ecological characteristics of the viruses-like particles considered
 116 in this study. Burst size was counted from transmission electron microscopy observations of
 117 host lytic events. ND: not detected.

118

119